Nov 7th, 12:00 AM - Nov 8th, 12:00 AM

Study on Distortional Buckling of Cold-Formed Stainless Steel Beams

Shuang Niu

Zhidong Zhang

Feng Fan

Wei-Wen Yu International Specialty Conference on Cold-Formed Steel Structures
St. Louis, Missouri, U.S.A., November 7 & 8, 2018

Study on Distortional Buckling of Cold-formed Stainless Steel Beams

Shuang NIU [1], Zhidong ZHANG [2], Feng FAN [3]

Abstract:

In the current research, distortional buckling of cold-formed stainless steel open-section beams was investigated. Four-point bending tests of eight C-section stainless steel beams, made of S30401 alloy, were carried out with global and local buckling precluded by careful design of specimen and test rigs. A detailed finite element model based on ABAQUS was developed and verified against test data. Parametric study was carried out with the verified model, covering four types of sections (C, Z, SupaCee, and SupaZed), three stainless steel alloys (S30401, S44330, S32101), and a series of section slenderness. A convenient method to identify distortional buckling point in either experimental or numerical study was discussed. Existing design formula for stainless steel and steel structure were assessed with the available data. Revised formula based on Direct Strength Method was proposed.

---

[1] Assistant Professor, School of Civil Engineering, Harbin Institute of Technology, Harbin 150090, PR China. <aniu216@126.com>
[2] Ph.D. student, Department of Civil Engineering, Johns Hopkins University, Baltimore, MD 21218, USA. <zhidongzhang@jhu.edu>
[3] Professor, School of Civil Engineering, Harbin Institute of Technology, Harbin 150090, PR China. < fanf@hit.edu.cn >

Introduction

Structural stainless steel sees a promising prospect in structural application, thanks to its advantages of aesthetic appeal, corrosion resistance, easy maintenance, retaining strength in fires and etc. Considerable progresses, as reviewed by Gardner(2005), Baddoo(2008) and Gedge(2008), were made during the past two decades in alleviating difficulties for stainless steel application, out of which one would emphasize the releasing and revision of design standards for stainless steel structure, and invention of cheaper yet stronger stainless steel alloys. However, there are still obstacles including high material price and incomplete knowledge about the effects of their nonlinear material properties on member behavior.

Cold-formed members feature high strength-to-weight ratio and therefore comprise a good choice for stainless steel structures. Design of such sections involves sectional (local and distortional) buckling behavior, which is further complicated by the profound nonlinear behavior of stainless steel (see Fig. 1). As the knowledge about sectional buckling advanced, it was found necessary to handle distortional buckling mode separately, which used to be treated indistinctly together with local buckling in existing research and design. Carefully designed test series were carried out by Yu & Schafer(2003,2006), to clearly separate and study local and distortional failure modes in cold-formed *steel* sections. As to *stainless steel* sections, local and distortional buckling were also involved in existing experimental studies such as Bredenkamp(1992) and Lecce(2006), but very rare study has clearly separate distortional buckling from local buckling and overall buckling. It is especially so for *stainless steel beams*.

In the current paper, distortional buckling behavior of open-section stainless steel beams were studied by a set of experiments featuring carefully designed specimen and loading rigs to rule out influence from local and overall buckling. The database was further augmented by parametric study using nonlinear finite element models, covering a wider range of section categories, material

categories, and section slenderness values. The available data such as ultimate bearing strengths were used in evaluating the accuracy of existing cold-formed stainless steel or steel member design formulas. Prediction formula based on Direct Strength Method (DSM) was subsequently proposed based on the data obtained.

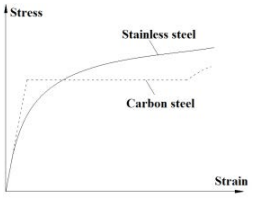

Fig. 1 Stainless steel and carbon steel stress-strain curves

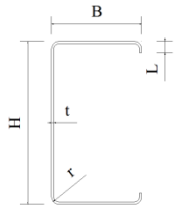

Fig. 2 Nomenclature for C section dimensions

Experiment Study

Materials

Test specimens were made from S30401 stainless steel sheets with a dimension of 4000mm x 1220mm x 1.74mm. The sheets were first laser cut into strips and then press-braked into test members. Material coupons from the virgin flat sheet and the cold-worked corner of specimens were tested. Flat coupons were cut from virgin flat sheets in the longitudinal (L), 45° diagonal (D) and transverse (T) directions, which were tested in both tension (T) and compression (C). Corner coupons were tested in tension using specially devised clamping rig. At least two coupons were tested for each case. Fig. 3 presents some typical stress-strain curves, in which "LT1" stands for the first ***L***ongitudinal coupon tested in ***T***ension.

Cross-sections and Specimen Geometry

Lipped-channel sections were designed, for which the elastic distortional buckling stress (f_{crd}) were kept lower than critical local buckling stress (f_{crl}). The nomenclature in Fig. 2 is used, where H, B, L, t, and r represent the

cross-section height, flange width, lip height, wall thickness, and corner external radius, respectively. The test members were labeled as A-1, A-2, B-1, B-2, C-1, C-2, D-1, D-2, respectively, with the actually measured member and cross-section dimensions listed in Table 1. Elastic buckling analysis was carried out with CUFSM, employing the actual measured section dimensions. The resultant ratio of f_{crd} /f_{crl} is listed in the last column of Table 1. Normalized distortional buckling slenderness (λ_d), as defined in Eqn. (1), is also listed in Table 1. An average proof yield stress in compression $f_{0.2}$= 242.29 MPa was used in the calculation.

$$\lambda_d = \sqrt{\frac{f_{0.2}}{f_{\mathrm{crd}}}} \qquad \text{Eqn.(1)}$$

Table 1. S30401 stainless steel C section specimen parameters

Member	Length(mm)	H(mm)	B(mm)	L(mm)	t(mm)	r(mm)	λ_d	f_{crd}/f_{crl}
A-1	3040	162.5	49.2	19.5	1.74	5	0.59	0.96
A-2	3040	162.4	49.4	19.3	1.74	5	0.59	0.96
B-1	3490	213.1	71.2	18.4	1.74	5	0.81	0.91
B-2	3490	212.9	72.0	18.3	1.74	5	0.82	0.90
C-1	3880	262.7	88.7	17.3	1.74	5	1.04	0.86
C-2	3880	260.2	89.5	17.8	1.74	5	1.03	0.87
D-1	3980	312.8	106.5	16.6	1.74	5	1.28	0.82
D-2	3980	311.0	106.1	17.1	1.74	5	1.25	0.84

Geometric Imperfections

Distortional buckling is sensitive to geometric imperfection according to Schafer(1999). A high precision imperfection measurement equipment was built up, which includes two high-precision tracks, a trolly running on them, and a program controlled step-motor that drives the trolly at a constant speed. As shown in Fig. 4, a specimen was placed under the track, and laser transducers mounted on the trolly run along the track while sampling distance from specimen surface at a constant rate. Imperfection information on eight measurement lines, as shown in Fig. 5, were collected for each cross-section.

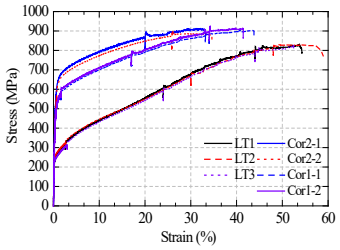

Fig. 3 Typical stress-strain curves for the coupon test (corner & flat sheet)

Fig. 4 Imperfection measurement device

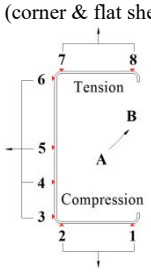

Fig. 5 Measurement locations on a C-section

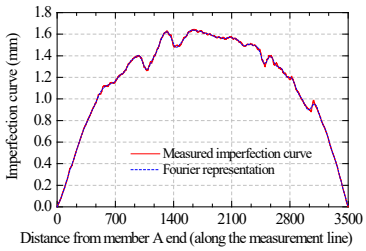

Fig. 6 #1 measurement line imperfection curve of B-2 member

As an example, the measured imperfection at measurement line #1 of B-2 specimen is presented in Fig. 6. The abscissa represents the location of cross-section along the length of the member, and the ordinate is the measured distance from laser transducer to the member surface. Fourier series representation (keep first 50 terms) of the imperfection line is also presented in Fig. 6, which follows the discrete imperfection data points very closely. The Fourier series representation curves were used for further analytical study for convenience.

Four-point Bending Test

Four-point loading set-up was used for bending test of the cold-formed stainless steel beams, see a sketch and actual photo of the set-up in Fig. 7 and Fig. 8. The set-up consists of a reaction beam, a mechanical jack, a spreader beam, two sets of links connecting the spreader beam and specimen, end supports and a series of lateral bracings. The mechanical jack was raised to produce two equal uplifting forces on the specimen. The rigs were set-up in this way to introduce

tensile force in the loading chain, which stabilize the loading system. Force sensor, displacement transducers, and strain gauges were used to record the load, deformation and strain distribution within the member during the test.

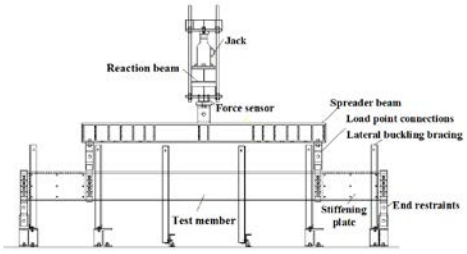

Fig. 7 Test set-up sketch

Fig. 8 Test set-up actual image

All of the test members developed distortional buckling deformation at the pure bending span. Take member B-1 as an example, the specimen deformation at peak load is shown in Fig. 9. Moment-deflection curves of all the specimens are presented in Fig. 10 and it could be found that the two nominally identical members have quite close deflection curve and ultimate capacity, which reflects the robustness of testing set-up and reproducibility of the test results.

Fig. 9 Obvious distortional deformation in compression flange at peak load of member B-1

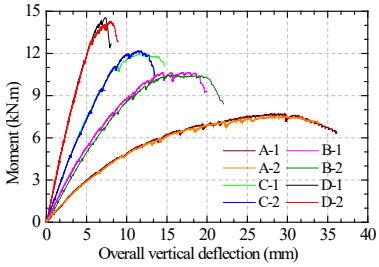

Fig. 10 Moment-vertical deflection curves of test members

Identification of the inelastic distortional buckling point has been a tricky work in thin-walled section tests. A most commonly adopted method was to monitor the buckling deformations of the compression flange, and then plot it against the applied load. Buckling onset point is then sought from such a curve, by finding a

transition point at which the slope of curve changes dramatically. However, this method turned out to be not a robust one. Transition point is obvious in some cases, but is hardly appreciable in many other cases.

During analysis of the strain data collected from the current tests, it was found that the strain at the compression corner plotted against the total load might be a more robust means for identifying the critical buckling point. Strain at the corner between compression flange and web was collected at mid-span section (see Fig. 11). Taking the absolute value of this strain as abscissa, and the force applied as ordinate, typical curves are shown in Fig. 12. It was found that there is a clear transition point in each load-strain curve marked by a dashed black circle.

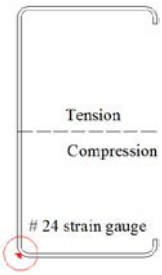

Fig. 11 Strain gauge position

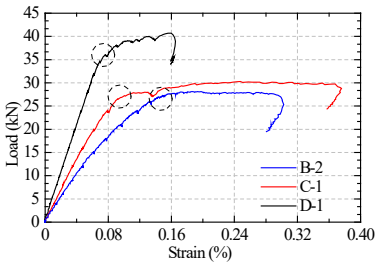

Fig. 12 B-2, C-1, D-1 member load-strain curves

Numerical Model and Calibration

Finite Element Model

A refined FE model was developed based on ABAQUS software package. This model simulates key details of the four-point load bending test as close as possible. The measured section parameters, material properties, and imperfection data were incorporated into this FE model.

Compression, tension and corner areas were distinguished in the C-section FE model, as indicated in Fig. 13. Static stress-strain curve was obtained by offsetting the actual coupon test curve to the static stress points obtained by repeatedly halting the coupon test. True stress-strain relationship was then

obtained. The nominal material parameters are summarized in Table 2. The Hill yield surface was used to consider stainless steel plates' anisotropy and the isotropic strain hardening criterion was adopted. Multi-linear curves sampled directly from the stress–strain curves were input into the FE model. It is found that cold-working has a profound effect on the material properties.

The reduced integration S4R shell element was adopted to simulate the member buckling behaviors. It was found that an overall mesh density of 5 mm could generate computational astringency and sufficient simulation accuracy.

Table 2. S30401 stainless steel material nominal mechanical properties

Coupon$_{(a)}$	$f_{0.01}$(Mpa)	$f_{0.2}$(Mpa)	f_u(Mpa)	E_0(Mpa)	ε_t– total elong %
LT	161.01	244.91	833.67	192.5	59.9
DT	166.51	242.01	818.63	187.9	61.7
TT	179.04	246.11	840.71	190.9	58.0
LC	147.94	242.29	\	194.3	\
DC	147.10	243.28	\	200.0	\
TC	183.71	258.61	\	202.2	\
Cor1	244.32	455.76	915.51	185.2	42.5
Cor2	249.23	516.18	920.53	190.7	38.5

(a) Coupon named as 'Cut direction Loading direction', 'LT' means a longitudinal tensile coupon test. 'Cor1' and 'Cor2' means the first and second batch cold-worked corner coupon tests respectively, and the second batch coupons were cut within the corner radius.

Four-point load set up modeling is presented in Fig. 14. Test member ends were simulated as hinges connected to ground with 'reference point' and 'multi-point coupling'. And the spreader beam was simulated as 'beam' connectors while the connection between spreader beam and the specimen was simulated as 'truss' connectors. The lateral bracings were simulated by restricting the out-of-plane translational freedom (U2) at a series of points, corresponding to points of restriction in actual specimen.

Fig. 13 C-section FE model with different material areas

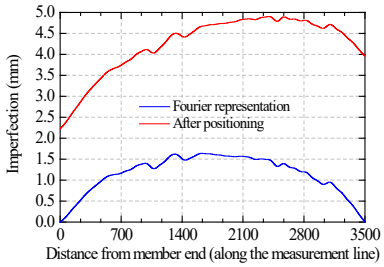

Fig. 15 Fourier representation of #1 line imperfection curve of B-2 specimen before and after data repositioning

Fig. 14 FE modeling of four-point load set up

Fig. 16 B-2 test member FE model after introducing imperfections (50x)

Home-made Matlab code was used to obtain Fourier representations of the imperfection data. Fig. 15 indicates the imperfection curve of #1 measurement line of B-2 test member before and after repositioning. Imperfection data from the eight measurement lines (see Fig.5) were then interpolated to obtain the imperfection data of the entire specimen. B-2 member FE model after introducing imperfection (magnified by 50 times) is shown in Fig. 16.

Finite Element Model Calibration

Good agreement was found between the test and FE modeling results in terms of ultimate bearing capacity and load-displacement curves. Table 3 shows that the average ratio of FE strength prediction to test strength is 0.97 with a standard deviation of 0.04. The test and simulation load-displacement curves are drawn in Fig. 17. It could be seen that the calibration FE model predictions are quite accurate.

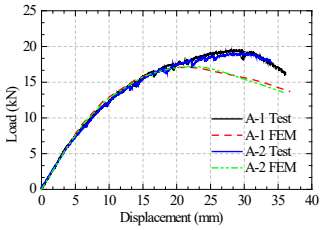

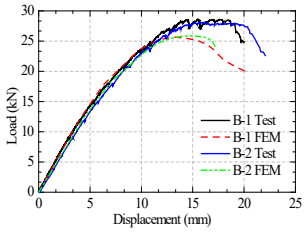

(a) Member A-1、A-2.

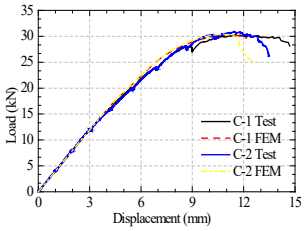

(b) Member B-1、B-2.

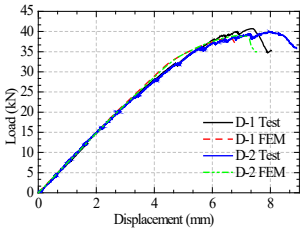

(c) Member C-1、C-2.

(d) Member D-1、D-2.

Fig. 17 Load-Displacement curves (load points displacement).

Table 3 Comparison of Test & FE modeling results of 304 stainless steel C-section members

Member	H(mm)	B(mm)	L(mm)	λ_d	M_{uFEM}(kN.m)	M_{uTest}(kN.m)	M_{uFEM}/M_{uTest}
A-1	162.5	49.2	19.5	0.61	6.75	7.28	0.93
A-2	162.4	49.4	19.3	0.61	6.79	7.21	0.94
B-1	213.1	71.2	18.4	0.84	9.55	10.17	0.94
B-2	212.9	72.0	18.3	0.84	9.64	10.33	0.93
C-1	262.7	88.7	17.3	1.07	12.02	11.73	1.02
C-2	260.2	89.6	17.8	1.06	11.99	11.93	1.00
D-1	312.8	106.5	16.6	1.31	13.75	14.35	0.96
D-2	311.0	106.1	17.1	1.29	13.95	14.00	1.00
						Avg	0.97
						St.Dev	0.04

Parametric Study

In the parametric study, section categories were extended to C, Z, SupaCee, and SupaZed, and more stainless alloys were used including S30401, S44330, S32101 stainless steel (by ASTM (2002), they are denoted as 304, 443, 2101 respectively in this paper). A number of plate thicknesses were also used to allow for practically large and small sections. 1.74mm, 3.0mm and 4.0mm section thickness were adopted for C and Z sections while 2.0mm, 3.0mm and 4.0mm section thickness were adopted for SupaCee and SupaZed sections. For each combination of alloy type, section category, and wall thickness of section, four sets of section dimensions were design to in accordance with distortional buckling slenderness values of 0.6, 0.85, 1.05 and 1.35 respectively. The member lengths were chosen so as that a pure-bending span (three times the distortional buckling half-wave length) and two 1200mm shear spans were obtained. Z section has the same section geometry nomenclature as C section, as indicated in Fig. 2. SupaCee section was referenced from Pham (2013) as

reproduced in Fig. 18(a). Again, SupaZed sections have the same nomenclature as SupaCee. There is an angle θ between the principle axis X-X and the axis 1-1 (perpendicular to the web). The loading directions of all the parametric study models were perpendicular to the principle axis X-X, as shown in Fig. 18(b).

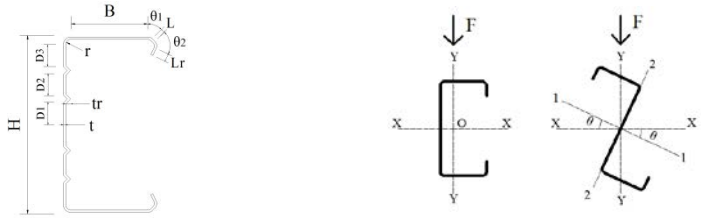

(a) Nomenclature of SupaCee section dimensions.

(b) Applied force direction.

Fig. 18 SupaCee section and applied force direction in parametric analysis models.

443 and 2101 stainless steel's mechanical properties in the parametric analysis models were referenced from experimental data in Niu (2014). Modeling imperfections necessitate buckle analysis of model. Distortional buckling mode resulted from buckling analysis were used as imperfection input data. The imperfection data was scaled to have a maximum amplitude of 0.15 × section thickness × distortional buckling slenderness as referenced from Niu (2014). All the parametric analysis models failed in a distortional buckling mode, resulting in a total of 138 successful simulations.

Analytic Study and Design Formula

Identifying Distortional Buckling Point Based on Compression Corner Strain

The same method as mentioned earlier for test data is checked here for parametric study results. The absolute strain value at the corner region between the compression flange and web was taken as the abscissa and the transverse load applied was taken as the ordinate. The load-strain curves of the representative cases were presented in Fig. 19. Each figure contains load-strain curves of those four sections of the same alloy, section category and wall

thickness (e.g. 304C-*-1.74 represents the four sections of 304 material, lipped channel section, and with a wall thickness of 1.74mm, section A~D corresponds to an increasing section slenderness of 0.6~1.35). It could be found that there exists an obvious transition point where the strain starts to develop faster in each load-strain curve. Therefore, monitoring the strain at the corner area between the compression flange and web seems a robust and effective way to identify the inelastic distortional buckling point. An increasing extent of post-buckling strength reserve were observed, after the buckling point, as the section slenderness increases.

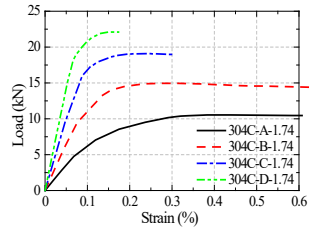

(a) 304-C section-1.74mm.

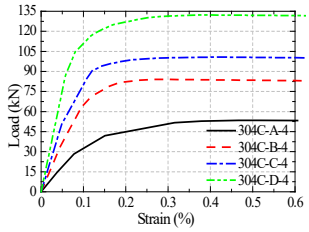

(b) 304-C section-4mm.

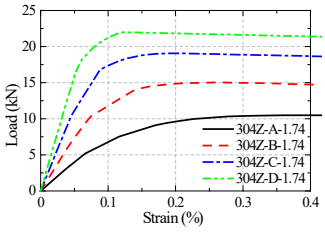

(c) 304-Z section-1.74mm.

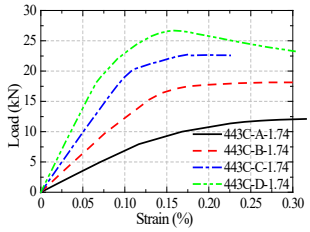

(d) 443-C section-1.74mm.

Fig. 19 Representative load-strain curves.

Design Formula

Experimental and simulation data on pure distortional buckling of stainless steel beams were collected in Fig. 20. All simulation data are labeled in the form of 'Alloy + Section Type', while test data are labeled with an additional postfix of '-Test'. The section types C, Z, SupaCee, and SupaZed are labeled respectively as 'C', 'Z', 'Cee', 'Zed'. For example, '304C' stands for the simulation data collected from the current paper, featuring 304 alloy and channel section.

Design curves related to distortional buckling of cold-formed stainless steel or steel members are also plotted in the Fig. 20. The distortional buckling design formula for pure bending members in Australian cold-formed steel structure design standard AS 4600(2005) is plotted as 'AS4600'. Niu (2014) proposed design formulas for 304 and 443/2101 stainless steel *beams*, which are plotted here as 'Niu-304' and 'Niu-443/2101' respectively. Lecce (2006) proposed austenitic and ferritic stainless steel *column* design curves, which are plotted here as 'Lecce-Austenitic' and 'Lecce-Ferritic'.

The DSM formula mentioned above can be expressed in a general form in Eqn. (2), where M_{crd} is the elastic distortional buckling moment, and the reference moment M_{ref} were generally assigned first yielding moment M_y (or sometimes overall buckling moment M_o) without exploring the plastic reserve of the cross-section. In the current research, overall buckling of member was fully braced and local buckling was virtually not triggered before distortional buckling. As a result, the sections studied were more capable in developing plastic deformation, and the section capacity were found way beyond the first yielding moment M_y. In the current study, plastic moment M_p was tried as reference moment (though it's generally believed that cold-formed steel sections hardly attain plastic moment M_p, the deep straining within flanges together with profound strain hardening of material in the current study has brought section capacity to a considerably higher level). Therefore, in Fig. 20 normalized strength M_d/M_p and normalized slenderness $\sqrt{(M_p/M_{crd})}$ were used to plot the data points.

$$\lambda_d = \sqrt{\frac{M_{ref}}{M_{crd}}} \qquad M_d = \begin{cases} M_{ref} & \lambda_d \le \lambda_0 \\ \left(\frac{a}{\lambda_d^{\,C}} - \frac{b}{\lambda_d^{\,2C}}\right) \times M_{ref} & \lambda_d > \lambda_0 \end{cases} \qquad \text{Eqn.(2)}$$

$$M_d = \begin{cases} M_p & \lambda_d \le 0.60 \\ \left(\frac{0.945}{\lambda_d^{\,0.947}} - \frac{0.197}{\lambda_d^{\,1.895}}\right) \times M_p & \lambda_d > 0.60 \end{cases} \qquad \text{Eqn.(3)}$$

$$M_d = \begin{cases} M_p & \lambda_d \le 1.00 \\ \left(\frac{1.487}{\lambda_d^{1.234}} - \frac{0.482}{\lambda_d^{2.469}}\right) \times M_p & \lambda_d > 1.00 \end{cases} \quad \text{Eqn.(4)}$$

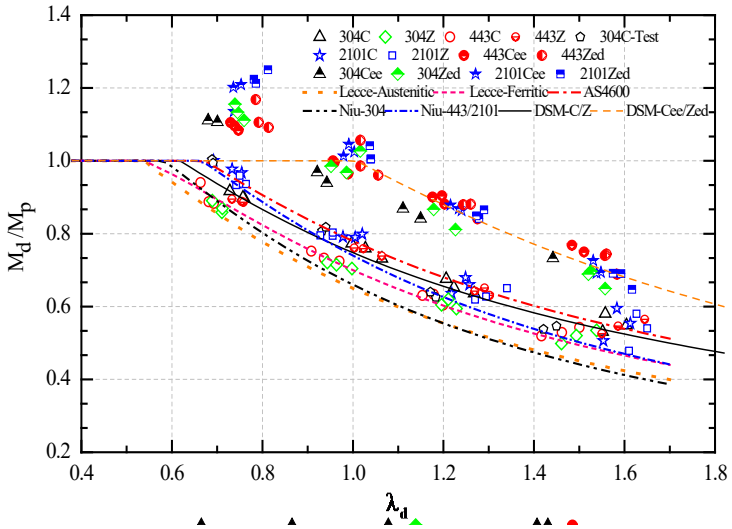

Fig. 20 Normalized strength–normalized slenderness data points of C / Z / SupaCee / SupaZed section models and design curves

From Fig. 20, it can be seen that SupaCee and SupaZed stainless steel beam capacities are systematically higher than those of C and Z section beams. The existing design curves are all significantly lower than SupaCee and SupaZed data points.

For C and Z section beams, 'Lee-Austenitic' and 'Niu-304' curves are constantly much lower than the data band. 'Lee-Ferritic' curve is following the data band quite well serving as a lower bound line. On the other hand, 'AS4600' curve is also following the data band and slightly lower than the upper bound line. 'Niu-443/2101' curve is passing through the data band, lying close to 'Lee-Ferritic' at higher slenderness region, and close to 'AS4600' at lower slenderness region. New design curve 'DSM-C/Z' was fitted based for the C and Z section beams, as expressed in Eqn. (3). The curve approximately follows the mid-line of the data band.

Another design curve 'DSM-Cee/Zed' was proposed for SupaCee and SupaZed beams, as expressed in Eqn. (4). The curve follows mid-line of the data band in the mediate to high slenderness range. At lower slenderness range, SupaCee and SupaZed beam data are way too high to be fitted by any DSM curve.

Conclusions

This paper presents eight four-point bending tests and a detailed FE model studying the cold-formed stainless steel beams featuring distortional buckling. Conclusions are as follows:

(1) Monitoring the strain at the corner between the compression flange and web of cold-formed stainless steel beam might be a robust method for identifying the inelastic distortional buckling load.

(2) The SupaCee and SupaZed section beams with the same material and slenderness level generally have higher normalized strength than the C and Z section beams. For a given section type, no appreciable deviation exists between the data points of different alloys. Instead, they are clustering and following a same trend line.

(3) Normalizing the distortional strengths with first yielding moment M_y result in way too high data points, while an attempt of using plastic moment as reference moment has resulted in reasonable fitting with existing design curves.

(4) Existing design curves were evaluated with experiment and simulation data points, 'Lee-Ferritic' and 'AS4600' curve were found close to the lower and upper bound of C and Z beam data, 'Niu-443/2101' curve was found lying between 'Lee-Ferritic' and 'AS4600', transiting from one gradually to the other. New design curves in DSM format were proposed separately for C/Z and SupaCee/SupaZed beam data.

Aknowledgement

This investigation was supported by National Natural Science Foundation of China (Grant No. 51508134), and the Fundamental Research Funds for Central Universities (Grant No. HIT.NSRIF.201676).

References

Baddoo, N. R. (2008). Stainless steel in construction: A review of research, applications, challenges and opportunities. Journal of Constructional Steel Research, 64(11), 1199-1206.

Bredenkamp, P. J., Van Den Berg, G. J., & Van Der Merwe, P. (1992, October). The lateral torsional buckling strength of cold-formed stainless steel lipped channel beams. In Eleventh International Specialty Conference on Cold-Formed Steel Structures (pp. 611-623).

Gardner, L. (2005). The use of stainless steel in structures. Progress in Structural Engineering and Materials, 7(2), 45-55.

Gedge, G. (2008). Structural uses of stainless steel—buildings and civil engineering. Journal of constructional steel research, 64(11), 1194-1198.

Lecce, M. (2006). Distortional buckling of stainless steel sections (Doctoral dissertation, Department of Civil Engineering, University of Sydney).

Lecce, M., & Rasmussen, K. (2006). Distortional buckling of cold-formed stainless steel sections: Finite-element modeling and design. Journal of Structural Engineering, 132(4), 505-514.

Niu, S. (2014). Interaction Buckling of Cold-Formed Stainless Steel Beams. The University of Sydney, Harbin Institute of Technology: Australia, China.

Pham, C. H., & Hancock, G. J. (2013). Experimental investigation and direct strength design of high-strength, complex C-sections in pure bending. Journal of Structural Engineering, 139(11), 1842-1852.

Schafer, B. W., & Peköz, T. (1999). Laterally braced cold-formed steel flexural members with edge stiffened flanges. Journal of Structural Engineering, 125(2), 118-127.

Standards Australia. (2005). Cold-formed steel structures. AS/NZS4600-2005, Sydney, Australia.

Yu, C., & Schafer, B. W. (2003). Local buckling tests on cold-formed steel beams. Journal of Structural Engineering, 129(12), 1596-1606.

Yu, C., & Schafer, B. W. (2006). Distortional buckling tests on cold-formed steel beams. Journal of structural engineering, 132(4), 515-528.